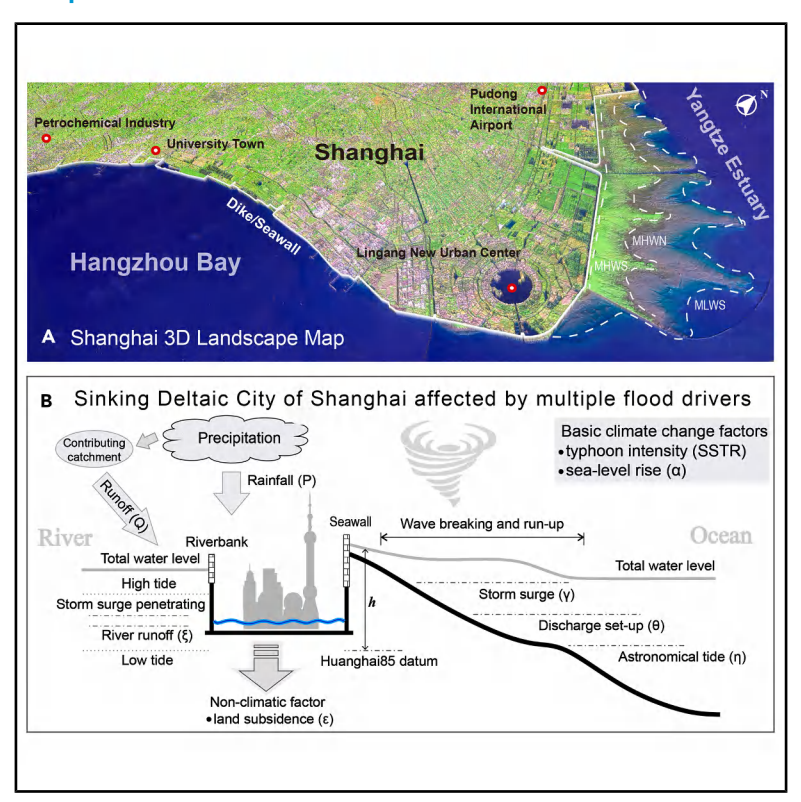
One Earth

Growing compound-flood risk, driven by both climate change and land subsidence, challenges flood risk reduction in major delta cities

Graphical abstract



Highlights

- A holistic model for assessing compound-flood risks at delta city scale is developed
- Flood risks in delta cities are increasing: up to 80% in Shanghai by 2100
- Rising sea levels and subsidence create a dangerous "polder effect" in delta cities

Authors

Min Zhang, Robert J. Nicholls, Jiahong Wen, ..., Stephen E. Darby, Shiqiang Du, Zhijun Dai

Correspondence

robert.nicholls@uea.ac.uk (R.J.N.), zjdai@sklec.ecnu.edu.cn (Z.D.)

In brief

Many flood-prone cities occur in deltas. Sea-level rise, land subsidence, and intensifying storm surges threaten larger and more frequent floods. While prior studies assessed individual flood components, none integrated the effect of all flood drivers. Using Shanghai as an example, we employed a dynamically-linked model to evaluate compound flooding. The possibility of a 200-year flood event potentially increases by up to 80% by 2100, far exceeding projections considering single flood components. We discuss the implications for other delta cities, including adaptation needs.



One Earth



Article

Growing compound-flood risk, driven by both climate change and land subsidence, challenges flood risk reduction in major delta cities

Min Zhang,^{1,9} Robert J. Nicholls,^{2,3,*} Jiahong Wen,¹ Amir AghaKouchak,⁴ Tjeerd J. Bouma,^{5,6} Stephen E. Darby,⁷ Shigiang Du,¹ and Zhijun Dai^{8,10,*}

SCIENCE FOR SOCIETY Delta cities are vital economic centers globally that are increasingly vulnerable to flooding from tropical and extratropical cyclones. Rising flood risks in these cities are driven by a combination of storm surge, river discharge, and precipitation occurring against rising sea levels and land subsidence. When multiple components are compounded, devastating floods can occur, as seen in Shanghai during Typhoon Winnie in 1997 and in Houston during Hurricane Harvey in 2017. This study presents a comprehensive model that integrates all relevant flood factors and their interactions for Shanghai. The interplay of storm-surge intensification, land subsidence, and sea-level rise significantly amplifies flood risk over time. Further, defense failure will lead to increasingly severe consequences (deeper, more extensive floods combined with poorer drainage), and this needs to be considered when planning adaptation to build flood-resilient cities.

SUMMARY

Low-lying deltas host some of the world's fastest-growing cities yet are exposed to floods driven by the compound actions of tide, storm surge, rain, and river flows. Most previous studies of compound floods are partial, while here, we estimate future compound floods in Shanghai for all relevant driving factors. We use a dynamically linked atmosphere, ocean, and coast model (AOCM) that incorporates all flood drivers, including sea-level rise (SLR), sea-surface temperature rise, and land subsidence. Simulations forced by baseline conditions and IPCC RCP2.6, -4.5, and -8.5 scenarios show that by 2100, the inundation extent of the 200-year event could increase by up to 80%, reflecting subsidence (34% [28%–41%]) and climate change (29% [20%–37%] due to SLR and 37% [26%–44%] due to more intense tropical storms), respectively. Land subsidence and SLR create a dangerous "polder effect" if defenses fail, which must be considered in adaptation in Shanghai and other deltaic cities.

INTRODUCTION

The world's low-lying low- and mid-latitude deltas are home to about 350 million people with rapidly growing cities and environments that are highly vulnerable to climate change. 1-3 These

deltas are frequently threatened by tropical and extratropical cyclones.^{3–6} Deltas also experience land subsidence that is often enhanced by human agency, especially in large cities like Shanghai.^{7,8} Compound-flood events—floods induced by the combined effects of two or more interacting sources, including

¹School of Environmental and Geographical Sciences, Shanghai Normal University, Shanghai 200234, China

²Tyndall Centre for Climate Change Research, University of East Anglia, Norwich NR4 7TJ, UK

³School of Engineering, University of Southampton, Southampton SO17 1BJ, UK

⁴Department of Civil & Environmental Engineering, University of California, Irvine, Irvine, CA 92697, USA

⁵Department of Estuarine and Delta Systems, Royal Netherlands Institute for Sea Research, 4400 AC Yerseke, the Netherlands

⁶Department of Physical Geography, Utrecht University, 3508 TC Utrecht, the Netherlands

⁷School of Geography and Environmental Sciences, University of Southampton, Southampton SO17 1BJ, UK

⁸State Key Laboratory of Estuarine and Coastal Research, East China Normal University, Shanghai 200062, China

⁹Yangtze River Delta Urban Wetland Ecosystem National Field Scientific Observation and Research Station, Shanghai 200234, China ¹⁰Lead contact

^{*}Correspondence: robert.nicholls@uea.ac.uk (R.J.N.), zjdai@sklec.ecnu.edu.cn (Z.D.) https://doi.org/10.1016/j.oneear.2025.101489





marine flooding (high tide, storm surge, and waves), fluvial flooding (river discharge), and pluvial flooding (rainfall) - are of particular concern. 9-13 Such compound events can have large social and economic consequences¹³ due to their amplified flood height and inundation extent 14 when compared to single-source floods. A well-known example of a devastating compound-flood event in Shanghai was Typhoon Winnie in 1997. 15,16 During this event, Winnie's storm-surge peak coincided with extreme river discharge and heavy precipitation, generating the highest recorded water level (WL; 5.99 m at Huangpu Park station; see Figures S1 and S2 for the location). The compound flood (Figure S3) killed and injured 248 and 5,412 people around the Yangtze delta, respectively, damaging more than 2,500 houses and causing 5.3 billion (1997 US\$) losses in Shanghai. 15 More recently, the 2021 Typhoon In-fa compound flood in Shanghai produced the third-highest WL ever recorded at Huangpu Park station (5.5 m), with an accumulated rainfall of over 200 mm, necessitating the emergency evacuation of 1.5 million people (even while coronavirus isolation laws were in place). These examples illustrate that compound floods pose a serious hazard to the populous cities located in the world's deltas.

Although compound-flood risk is almost certain to increase in a warming world with rising sea levels3,5,13,14 and land subsidence, 8,16,17 the interaction of the full range of compound-flood drivers has not often been investigated in detail for deltaic cities. This knowledge gap reflects the fact that compound flooding is a complex phenomenon driven by intertwined climatic and nonclimatic forcings. 11,13,18 Compound-flooding studies to date typically consider the interaction of two drivers, for example, hydrologic and oceanic drivers, such as storm surge with astronomical tides, 18 storm surge with extreme waves, 19 storm surge with heavy precipitation, 13,20 and storm surge with high river inflow. 11,12 This approach ignores important non-climatic components (e.g., land subsidence) that are significant in urban delta environments. Moreover, with some notable exceptions, 21,22 such as considering storm surge with sea-level rise (SLR)^{23,24} or storm surge with land subsidence, 16,17 most prior studies do not consider the overall changing nature of the risk factors as the environment changes through time. In particular, anthropogenically driven climate change affects (1) sea-surface temperature rise (SSTR),25 which in turn impacts the magnitude and frequency of tropical storms, 5,26 and (2) SLR,27 which progressively increases the baseline water elevation on which a flood event is superimposed-contributing to hydrologic and oceanic drivers of coastal flooding. These interactions are often compounded by (3) land surface subsidence (LSS)²⁸ as a non-climatic component affecting most rapidly urbanizing deltas, 29-31 especially in big cities.^{8,32} Indeed, subsidence can be a significant factor in progressively increasing exposure to flooding,8 even under a stable climate.

The large populations and economic importance of the world's deltas provide a compelling need for robust assessments of compound floods and their changing risks, 1,2,8 particularly in the densely populated deltaic cities that widely depend on dikes for their safety. 32–34 In Shanghai, for instance, a 510 km dike system safeguards land largely reclaimed from marshes/tidal flats, with an average city elevation just above high-tide levels (2–3 m). 16,35,36 Many other deltaic cities depend on dikes to keep them dry and habitable today, such as New Orleans, Rotterdam,

Amsterdam, and Bangkok. 6,21,30,31,33 Moreover, there is the risk of "polder floods," where dikes fail and the flood water cannot drain from these low-lying areas by gravity. 21,34 Hence, submergence would persist well beyond the extreme flood event until the dikes were repaired and the water pumped out, as happened in New Orleans after Hurricane Katrina. 19,37,38 With rising sea levels and ongoing LSS, dikes need regular raising, but the residual risk of dike breaching and/or overtopping under extreme conditions still threatens significant and potentially catastrophic socio-economic consequences. 30,39 Therefore, in these lowlying cities, dike failure acts as a critical threshold-once overtopped, even moderate storms can become suddenly catastrophic. 30,33 Here, we explore the "polder effect" that occurs in subsiding deltaic cities that rely on flood defenses, where elevation declines relative to the tidal frame so that if floods occur, the water cannot flow away by gravity afterward. In the future, continued subsidence combined with climate-induced changes such as SLR will further exacerbate the polder effect. Hence, in addition to the joint interactions between coastal, fluvial, and pluvial flood drivers, the distinct topographical effects of dikes and their longer-term interactions with climate-driven (e.g., SSTR and SLR) and non-climatic (e.g., subsidence) drivers must be considered. Understanding all these complex interactions, including the polder effect, today and how they will evolve into the future, is key to assessing potential disasters and managing these risks in deltaic cities.

To address this research gap, we couple a fully integrated atmosphere, ocean, and coast model (AOCM) with established dike wave-overtopping models, 35,36,39,40 considering scenarios of all component drivers and their interactions. We focus on the case of Shanghai in the Yangtze delta, an example of one of the most populous and vulnerable low-lying deltaic cities in the world.⁴¹ We reproduced the ten historical super-typhoons that caused Shanghai's worst flood losses over the past 50 years (see Figure S1 and Table S1). These provide analogs to project conditions in 2035, 2050, and 2100 under IPCC RCP2.6, -4.5. and -8.5 emission pathways⁴² that consider storm intensification, SLR, and LSS. Our results highlight how extensive dike systems and low-land elevation create a pronounced polder effect, magnifying flood hazards. We then consider the implications for other urban areas located on estuaries and deltas by comparing our findings from Shanghai with a high-level analysis of compound hazards across 40 major estuarine/deltaic cities worldwide, 30,32,43 situated in vulnerable regions such as the Mekong, Chao Phraya, Irrawaddy, and Ganges-Brahmaputra-Meghna (GBM) deltas.31

RESULTS

Methods summary

We developed a fully coupled AOCM that integrates all compound-flood drivers (SSTR-enhanced storm surge, tide, river discharge, precipitation, SLR, and LSS) and their interactions to project future compound flooding in Shanghai. First, the ocean model was forced with SLR trajectories and storm-surge intensification under IPCC RCP2.6, -4.5, and -8.5 scenarios (Table 1) and run for the 40-year baseline: 1979–2020. The baseline provided boundary conditions for the coast model, together with significant wave heights (SWHs) and WLs representing the

Þ	0
7.	ne
D	П
	2
	5

	Long-term climate change		Extreme hydrometeorological factors			Anthropogenic factors	
Group parameters	SSTR (°C)	SLR (m)	Storm strengthening	Precipitation	River discharge	LSS	Coastal defenses
Real case ^a	27	0	Typhoon Winnie	measured	measured	2010	1997
Control cases ^a	27	0	ten historical compound events	measured	measured	2010	1998
Scenario cases ^b							
2035/2050/2100							
RCP2.6 mean	+0.3/+0.4/+0.8	+0.11/+0.18/+0.42	+3%/+4%/+5%	+3%/+5%/+10%	+3%/+5%/+10%	projected 2035 mean/projected 2050 mean/ projected 2100 mean	projected 2035 mean/ projected 2050 mean/ projected 2100 mean
RCP4.5 mean	+0.5/+0.8/+1.8	+0.13/+0.2/+0.52	+4%/+6%/+10%	+5%/+8%/+15%	+5%/+8%/+15%		
RCP8.5 mean	+0.7/+1.2/+3	+0.16/+0.29/+0.72	+6%/+9%/+18%	+7%/+10%/+20%	+7%/+10%/+20%		
RCP4.5 high	+0.9/+1.5/+3.2	+0.19/+0.27/+0.67	+7%/+10%/+19%	+9%/+13%/+25%	+9%/+13%/+25%		
RCP8.5 low	+0.5/+0.8/+2	+0.11/+0.18/+0.48	+5%/+7%/+12%	+5%/+8%/+15%	+5%/+8%/+15%		
RCP8.5 high	+1.2/+1.8/+4	+0.25/+0.35/+0.92	+9%/+14%/+25%	+10%/+15%/+30%	+10%/+15%/+30%		
Sensitivity test cases	S ^C						
2100							
Test 1	-	0	+25%	+30%	+30%	projected 2100 mean	projected 2100 mean
Test 2	_	+0.92	0	+30%	+30%		
Test 3	_	+0.92	+25%	0	+30%		
Test 4	-	+0.92	+25%	+30%	0		
Test 5	_	+0.92	+25%	+30%	+30%	2010	1998
Test 6	-	+0.92	+25%	+30%	+30%	projected 2100 low	projected 2100 low
Test 7	-	+0.92	+25%	+30%	+30%	projected 2100 mean	projected 2100 mean
Test 8	_	+0.92	+25%	+30%	+30%	projected 2100 high	projected 2100 high

^aThe real and control cases reproduce the historical typhoon-induced compound flood forced by observations. The real case with the 1997 defenses (dikes/seawall) is used for model validation. The control case of ten historical typhoons with the 1998 dike/seawall configuration is the reference case, providing the baseline for the design of the future scenarios.



bScenario cases explore the possible exacerbation of flooding in Shanghai in 2035, 2050, and 2100 based on a number of published scenarios, including the IPCC long-term climate scenario of global SSTR and SLR, extreme hydrometeorological factors of SSTR-enhanced storm strengthening, typhoon-induced precipitation, extreme river discharge, and anthropogenic factors of land and dike/seawall subsidence, as described in detail in Note S2.

^cThe sensitivity test cases are designed for sensitivity analysis of non-compound floods, e.g., leaving the components of SLR, storm surge, heavy rainfall, extreme river discharge, and land (dike/seawall) subsidence out of all compound floods, respectively. The uncertainty of land (dike/seawall) subsidence is tested with low, medium, and high scenarios, as described in detail in Note S2.



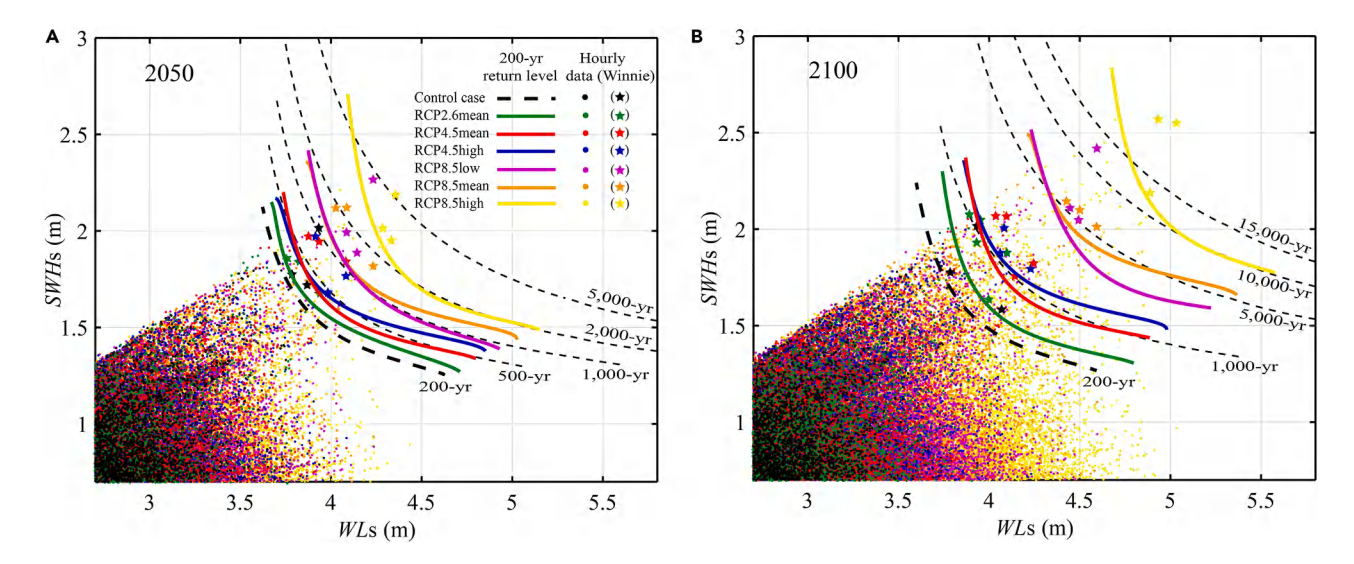


Figure 1. Projection of future compound-flood event evolution in Shanghai

The forecast is based on the 10 super-typhoons shown in Figure S1, with projections for (A) 2050 and (B) 2100 derived from a joint probability analysis³⁴ of water levels (WLs) and associated significant wave heights (SWHs) at Wusong station (see Figure S2B for the location), using data obtained from a 40-year simulation, 1979–2020. The black scatter points show the hourly WLs-SWHs over the past 40 years, with black dashed lines representing the current estimated recurrence intervals, which will become more frequently exceeded in the future (as indicated by the colored points and lines). The specific example of Typhoon Winnie and its future evolution is illustrated, marked with stars. Winnie was the most severe typical compound-flood event experienced by Shanghai in the past four decades. Detailed parameters used for the control case and future scenarios are provided in Table 1 and the methods.

present-day and future 200-year return levels (Figure 1). Joint extreme-value analysis (Copula; Note S1) supplied the combined WL and wave scenarios (Figure 1). We then simulated ten historic super-typhoon tracks comparable to Typhoon Winnie, varying river discharge and precipitation to define the range of plausible futures (Figure S1; Table S1). For each track, the full AOCM was rerun for 2035, 2050, and 2100 using the updated forcing of 200-year return levels, embedding scenariospecific SLR, storm-strength amplification, and LSS—including consequent dike-crest lowering (see Table 1 and methods). The simulations yield inundation extents and exposure metrics (e.g., people and assets), revealing how a 200-year event escalates over the 21st century under climate- and subsidence-driven changes.

To compare Shanghai with other deltaic urban centers, we created a global ranking of compound-flood hazards for 40 significant estuarine/deltaic cities with at least one major river. 30,32,43 Because detailed terrain and dike-height data are rarely available worldwide, we derived a simplified, linearized extreme WL method that captures the combined influence of the aforementioned six drivers—SSTR-enhanced storm surge, tide, river discharge, precipitation, SLR, and LSS. For each city, we evaluated the 200-year return level of every driver and combined them probabilistically into a dimensionless compound-flood index (CFI), which serves as a proxy for extreme WL, h(x,t) (see Equation 1 in methods). This unified metric highlights inter-delta differences and situates Shanghai's compound-flood hazard within a consistent global context.

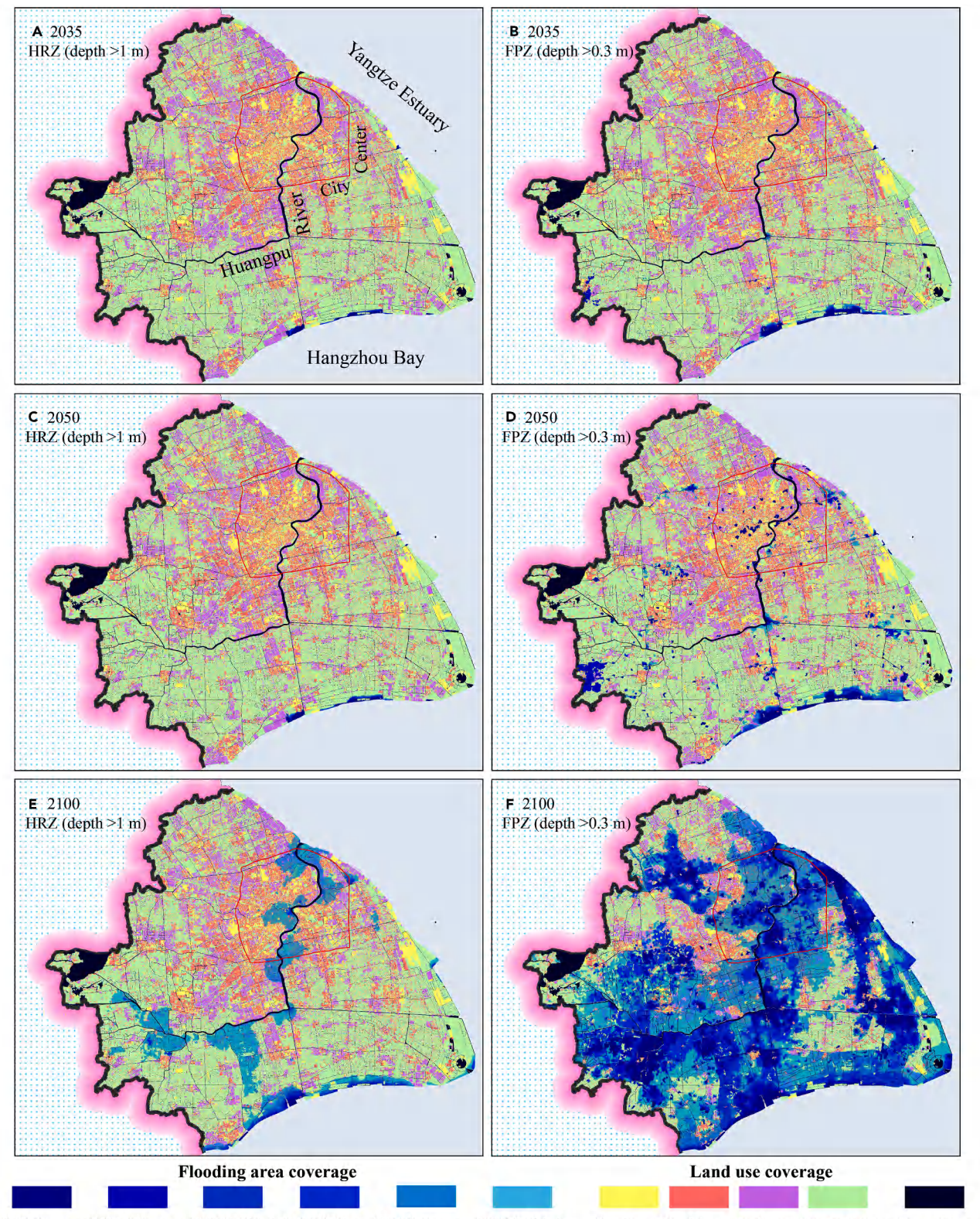
Flood extent of major compound events in Shanghai by 2100

The analysis projects a significant increase in the flood-prone zone (FPZ)—which is defined as an inundation depth exceeding

0.3 m (Figure 2). Specifically, our extreme scenario (RCP8.5-high) projections indicate that the extent of the FPZ will increase by 1.9% (or 70–108 km²; the numbers in parentheses are the 5%–95% bounds and are the same hereafter) of the urban area by 2035, 5.3% (or 228–344 km²) by 2050, and 33.7% (or 505–3,138 km²) by 2100, with the precise change depending on the future climate and non-climate factors. Similarly, the extent of the high-risk zone (HRZ) within the FPZ—which is defined as an inundation depth exceeding 1 m—increases by 0.15% (or 3–16 km²) of the urban area by 2035, 0.6% (or 8–53 km²) by 2050, and 4.8% (or 9–509 km²) by 2100. The HRZ mainly affects both sides of the Huangpu River and the southern coastal area north of Hangzhou Bay (Figures 2A–2C and 2E). Detailed projections of flood extent and depth are provided in Figures S4–S7.

These floods may have devastating consequences in terms of future social safety and property damage, especially after 2050, when the flood-exposed area expands substantially (Figure 3). The total population of Shanghai in 2010 was 22.4 million (Figure S8). If the present population growth rate of 1.3% is assumed to continue, 41 the city's population would reach 30.7 million in 2035, 37.6 million in 2050, and (maybe) 71.6 million in 2100. Under this scenario, approximately 0.06 (0.03-0.15), 0.2 (0.1-0.5), and 15.9 (9.9-39.1) million people will be exposed within the FPZ and 0.0015 (0.0007-0.003), 0.005 (0.002-0.01), and 4.3 (2.7-10.6) million will be exposed within the HRZ by 2035, 2050, and 2100, respectively. In the FPZ, industrial areas are more exposed than residential and business-service areas (Figure 3), comprising 10 (7-26), 6 (4-15), and 3 (2-7) km² by 2050 and 182 (114-448), 178 (111-436), and 88 (55-216) km² by 2100, respectively. It is evident that floods along the Huangpu River are more damaging (exposing 75%–85% of the population and 55%-75% of properties to the FPZs) than floods on the open





RCP2.6mean RCP4.5mean RCP4.5high RCP8.5low RCP8.5mean RCP8.5high

Business Residence Industry No building River&Lake

(legend on next page)





coastline (Figures 3C-3E and 3G). This is because the population and business districts are concentrated along the Huangpu River (Figure S8), which is the largest river in Shanghai presently lacking sluice-gate protection. However, the critical infrastructure projected to be flooded in the HRZs is located entirely along the open coast by 2050 and comprises 50%-65% of losses by 2100 (Figures 3D-3F and 3H). Threatened infrastructure includes Pudong International Airport and many polluting enterprises (e.g., the petrochemical industry and wastewater treatment industry are all located along the coast; Figure S2B), as well as the Qinshan Nuclear Power Plant, although this has additional protection that is not assessed in this analysis. Therefore, floods along the Huangpu River tend to result in large-scale economic and human losses, while floods on the open coast are less severe but still have important consequences, such as the release of pollutants.

Influence of climate and non-climate change factors

Evaluating flood events in 2050 and 2100 shows that SSTR increases SWHs, while rising sea level, higher surges, and river discharges raise WLs (Figure 1). Overtopping is predicted to occur when the combined WLs exceed the 4.2 m local dike height (at Wusong station). Storm-surge WLs increase under future conditions, with the specific magnitude of the increase depending both on future climate projections and SLR (Figure 1). For example, joint probabilistic analysis shows that the WL in Typhoon Winnie was a 1-in-200-year return period level at the Huangpu River entrance (i.e., at Wusong station), but by 2100, it is projected to reach a 1-in-1,000-year or even a 1-in-10,000year event (in 2020 terms) under the RCP4.5-mean scenario (0.52 m SLR and 1.8°C SSTR) and the RCP8.5-high scenario (0.92 m SLR and 4°C SSTR), respectively (Figure 1B). In addition to increased extreme WLs, the return period of a given WL will be reduced for each current typhoon category, making extreme events both more frequent and more severe over the 21st century.

For pluvial floods, rainfall and runoff are estimated to generate more than half of the total floodwater volume (Table S2). However, as rainfall affects the whole city, pluvial runoff alone mostly tends to cause shallow flooding over large areas where h < 0.3 m (Figures S4–S6). The main impact of pluvial flooding, therefore, is exacerbating waterlogging when combined with compound WLs of coastal and/or fluvial overtopping (Figure S7). The present dike/seawalls and riverbank defenses start to overtop at numerous low-lying locations under the mean-high scenarios of RCP4.5 and RCP8.5 by 2050, and almost all present dikes/seawalls (>90%) and half of the present riverbank defenses (43%) are ineffective in protecting the urban area of Shanghai under the RCP8.5-high scenario by 2100 (Figure S7).

In addition to the influence of anthropogenic climate change factors (i.e., SLR and SSTR), LSS also makes a large contribution to the increased hazard. LSS in Shanghai has been substantial since the 1920s, and this is expected to continue, as shown in

Note S2. Subsidence influences flooding in two ways: (1) it lowers riverbank and coastal defenses, making overtopping more likely (see Figure S7), and (2) it lowers ground levels, making floods deeper when they do occur. Sensitivity tests (Table 1) reveal that the combined influence of climatic (SLR and SSTR) and non-climatic (LSS) factors significantly amplifies compound-flood hazards, increasing by 4–6.5, 3.5–5, and 3–3.2 times in the late 21st century relative to changes in the single flood factor of SSTR-enhanced storm strengthening, LSS, and SLR, respectively (Figures S9–S11; Table S3). This amplification may vary by approximately 10%–15%, depending on uncertainties across low- to high-impact human intervention scenarios on land subsidence (Figures S14–S16).

SSTR-enhanced storm surge is the strongest driver of flood risk

According to the results of our extreme scenarios model, compound-flood hazard will be significantly amplified in the late 21st century due to the combined effects of anthropogenic climate change (SLR and SSTR) and non-climatic processes (LSS). The combined effects of marine, fluvial, and pluvial mechanisms contribute to increases of the extreme floodwater volume in 2100 by 41% (98-812 M·m³), 36% (220-497 M·m³), and 23% (86–422 M·m³), respectively (Table S2). In terms of the relative importance of each compound driver in contributing to these floodwater volumes, the long-term changes in SSTR-enhanced storm strengthening, LSS, and SLR contribute approximately 37% (26%-44%), 34% (28%-41%), and 29% (20%-37%), respectively. Omitting any of these components leads to substantial underestimation of both the FPZ and HRZ extents. Omitting one component at a time causes SSTR-enhanced storm surge underestimates by 75%-85%, LSS underestimates by 71%-81%, SLR underestimates by 67%-68%, river discharge underestimates by 47%-51%, or precipitation underestimates by 10%-27% (Figures S9-S13; Table S3).

Our extreme scenarios projections also suggest that, regardless of the non-climatic factor LSS, climate-change-enhanced marine flooding is more challenging under SSTR than SLR by 2100. This is because the recognized FPZ extent forced by future changes in SSTR (1.8°C-3°C) is projected to increase 1.7-2.0 times under the optimistic emissions scenario RCP4.5 mean and the high-end emissions scenario RCP8.5 mean, compared with "only" an increase of 1.1 times forced by SLR (0.52-0.72 m) under the same two emissions scenarios. Meanwhile, the corresponding changes in HRZ exhibit increases in extents of approximately 2.1-2.9 times for SSTR and 1.8-2.5 times for SLR for the driving factors investigated (see Table S2). Moreover, our sensitivity analysis also reveals a more profound influence of SSTR than SLR on extreme non-compound floods by 2100. For example, excluding SSTR-enhanced storm surge from the RCP8.5-high scenario reduces the FPZ (or HRZ) extent by 2,310-2,950 (or 340-423) km², while excluding SLR "only" reduces the FPZ (or HRZ) extent by 1,890-2,350 (or 311-382) km² (Table S3; Figures S9 and S10).

Figure 2. Maximum inundation extent of future extreme compound floods

(A–F) Flood-prone zone (FPZ; depth > 0.3 m) and high-risk zone (HRZ; depth > 1 m) inundation extents for future extreme compound floods (200-year return period levels) in the years 2035, 2050, and 2100. Boundary conditions and model configurations for the scenarios are listed in Table 1 and the methods. Land use/coverage is classified into five types: business-service, residence, industry, no buildings, and water area.



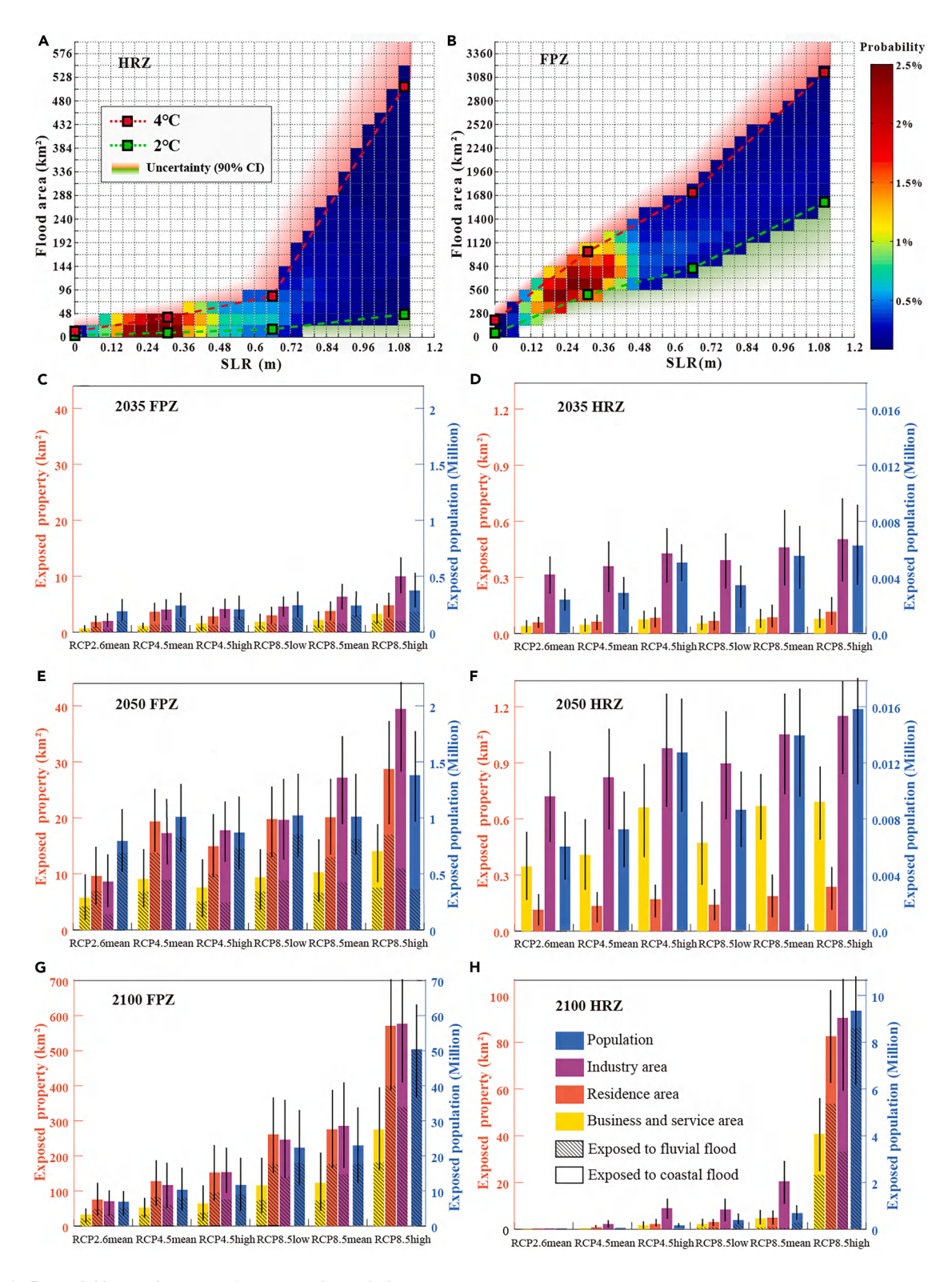
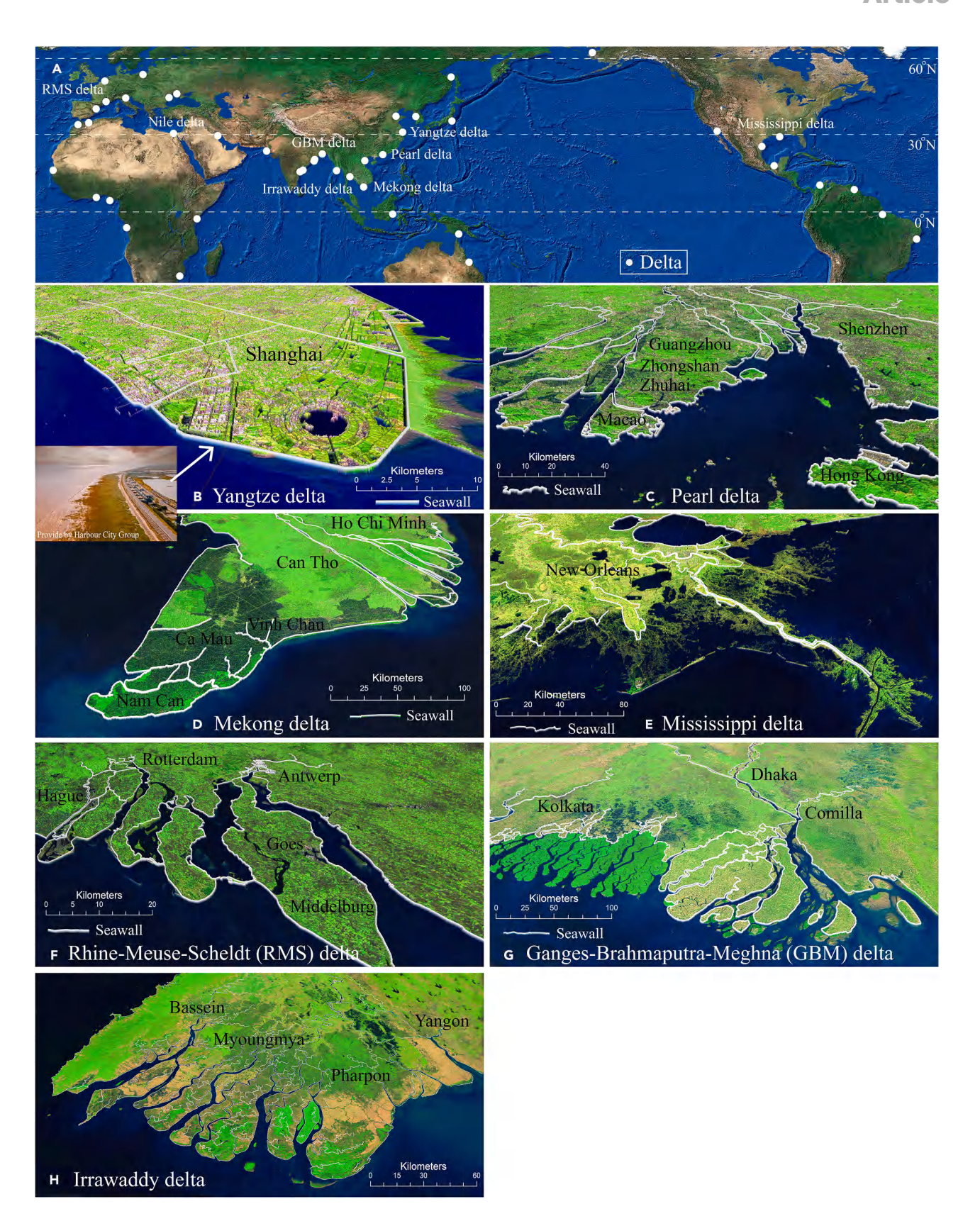


Figure 3. Potential losses in terms of assets and population

(A and B) Expected flood area (note difference in scales) and occurrence probability for the flood-prone zone (FPZ; depth > 0.3 m) and high-risk zone (HRZ; depth > 1 m) under the effects of anthropogenic climate change, including sea-level rise (SLR) and sea-surface temperature rise (SSTR). The subtle green and pink shading indicates flood area uncertainty (90% confidence interval) based on SSTR of 0.8°C–4.8°C for the 2100 projection. 44,45 (C–H) Expected population and assets (note the difference in scales) exposed in the FPZ and HRZ in the years 2035, 2050, and 2100 under future scenarios with

5%–95% bounds based on the probability distribution of SLR and SSTR projections.







Implications for major estuarine/deltaic cities across the globe

Deltas, formed by the deposition of sediment carried by rivers into the sea, are typically low-lying regions, and in mid- and low latitudes, they support dense populations, including large cities, due to their fertile land. Many of the world's major deltas are situated at the mouths of large river basins, such as the Yangtze, Pearl, Mekong, Mississippi, Rhine-Meuse-Scheldt (RMS), GBM, and Irrawaddy deltas (Figures 4 and 5A). These regions are predominantly within the concentrated influence zone of active cyclone tracks. Hence, cities in these areas are vulnerable to compound flooding, which can result from the combination of storm surge, tides, river floods, and precipitation. Additionally, these cities are typically built on unconsolidated sediments and are prone to LSS, exacerbating the impacts of SLR caused by climate change.

We assessed the compound-flood hazard for 40 major estuarine/deltaic cities, home to over 300 million people, and found that 90% of these cities are located in active tropical and extratropical cyclone-prone regions (Figure 5A). These cities are highly vulnerable to compound coastal, fluvial, and pluvial flooding. Based on a comprehensive analysis of 200-year return levels for the aforementioned six flood drivers (Figures S17-S22), we ranked these cities by their vulnerability to compound-flood hazards using our CFI metric (Figure 5B). Our findings highlight the high risk faced by cities such as Yangon, Shanghai, Dhaka, Ningbo, Karachi, Guangzhou, and New Orleans, as shown in Figure 4 and in Table S4. Shanghai is ranked number 2, while 7 of the 9 cities (in Table S4) are in the top 11 for high compound-flood risks, as shown in Figure 5B, indicating the importance of compound events in flooding across deltaic cities. The results emphasize the urgent need for tailored flood adaptation strategies in high-risk cities. The findings also underscore the varying levels of risk across global deltaic cities and suggest that even cities with relatively lower flood risks may face increased vulnerability due to rising sea levels, land subsidence. and tropical cyclone intensification. These findings highlight the importance of strengthening flood resilience in vulnerable urban centers globally, including through enhanced coastal defenses and integrated risk management strategies.

DISCUSSION

Deltaic cities are home to hundreds of millions of people and are critical lynchpins in national and international networks and economies. ^{1,2} Meanwhile, deltaic cities worldwide are facing escalating flood threats driven by storm surges, high river discharge, and heavy precipitation—all compounded by rising sea levels and land subsidence. ¹⁰ Most analyses consider these different flood drivers independently, ignoring their potential compounding effects. ^{4,11–13,16,18,20,24} Our research presents a robust and holistic model, which is a dynamically linked AOCM, that considers scenarios of all these components and their interactions. The analysis demonstrates that large com-

pound-flood events in Shanghai will grow dramatically over the next 75 years, threatening most of the city unless defenses are significantly improved. Subsidence, SLR, and more intense storms, the latter driven by increasing ocean surface temperatures, are key drivers. Other deltaic cities share similar geographic and environmental challenges and risks to Shanghai (Figures 4 and 5). Continued LSS and SLR are creating a dangerous polder effect in many delta urban centers, making Shanghai and other, similar urban areas more vulnerable to future compound floods. Policymakers and urban planners must advance flood resilience through multi-layered defense systems and community-based adaptation efforts.

Understanding the drivers of compound floods in Shanghai

Any flood is dangerous for low-lying delta urban areas, and a higher compound flood generated by a combination of multi-hydrometeorological factors is more dangerous due to the higher WLs that result. 11,13,18,36 Compound floods already threaten Shanghai, as shown by Typhoon Winnie and other similar storms, while Figure 5 suggests that these issues are widespread across deltaic cities. Our model of extreme scenarios simulation under IPCC RCP2.6-8.5, with probabilistic analysis based on 40-year compound WLs, reveals that the compoundflood threat in Shanghai will be substantially amplified over the 21st century due to the enhancement of multi-hydrometeorological drivers and slow-onset climatic and non-climatic factors. This is especially true for large amounts of warming and SLR. For example, the predicted flood extent for extreme compound floods under the RCP8.5-high scenario would increase by up to 80% by the year 2100. The non-climatic factor, LSS, accounts for about 34% (28%–41%) of this flooding, whereas the climatic factors, SSTR-enhanced storm strengthening and SLR, contribute about 66% (46%-81%).

A key finding of our study is that many estuarine/deltaic cities worldwide have constructed dikes as they have expanded and often subsided to protect their economically and demographically significant but low-lying areas. 30,33,35 This resulting polder effect makes deltaic cities highly vulnerable to dike failure, which in turn increases the impact of compound floods. Shanghai's coastline is exposed to ocean hazards on three sides, with Taihu Lake forming the fourth boundary (Figure S2). As such, the city comprises a low-lying polder (Figure 4B), like the Netherlands or New Orleans, where dikes are crucial for keeping the city dry and habitable. 6,30,33,37 However, as the city's dependence on flood defenses grows, if failure occurs, the resulting flood depths and damage also increase. Fewer but larger flood events may be expected as coastal defenses are raised and WLs rise. 32 Although Shanghai is generally well protected by dikes, seawalls, and riverbank defenses (Figures 4B and 6B), land subsidence reduces their height and effectiveness over time, 16 amplifying flooding as sea levels and wave heights rise. This dynamic could lead to polder flooding, where floodwaters remain trapped and the city stays submerged for prolonged periods until the

Figure 4. Typical landscapes of large deltas

(A) Examples of important deltas worldwide and (B–H) the landscapes of selected large deltas with cities located in low- and mid-latitude regions. The low-lying delta geomorphology is commonly protected by dikes, both on the coast and along the rivers. Climatic and non-climatic drivers, including sea-level rise and land subsidence, exacerbate the future risk of flooding and dike failure (breaching or overtopping).



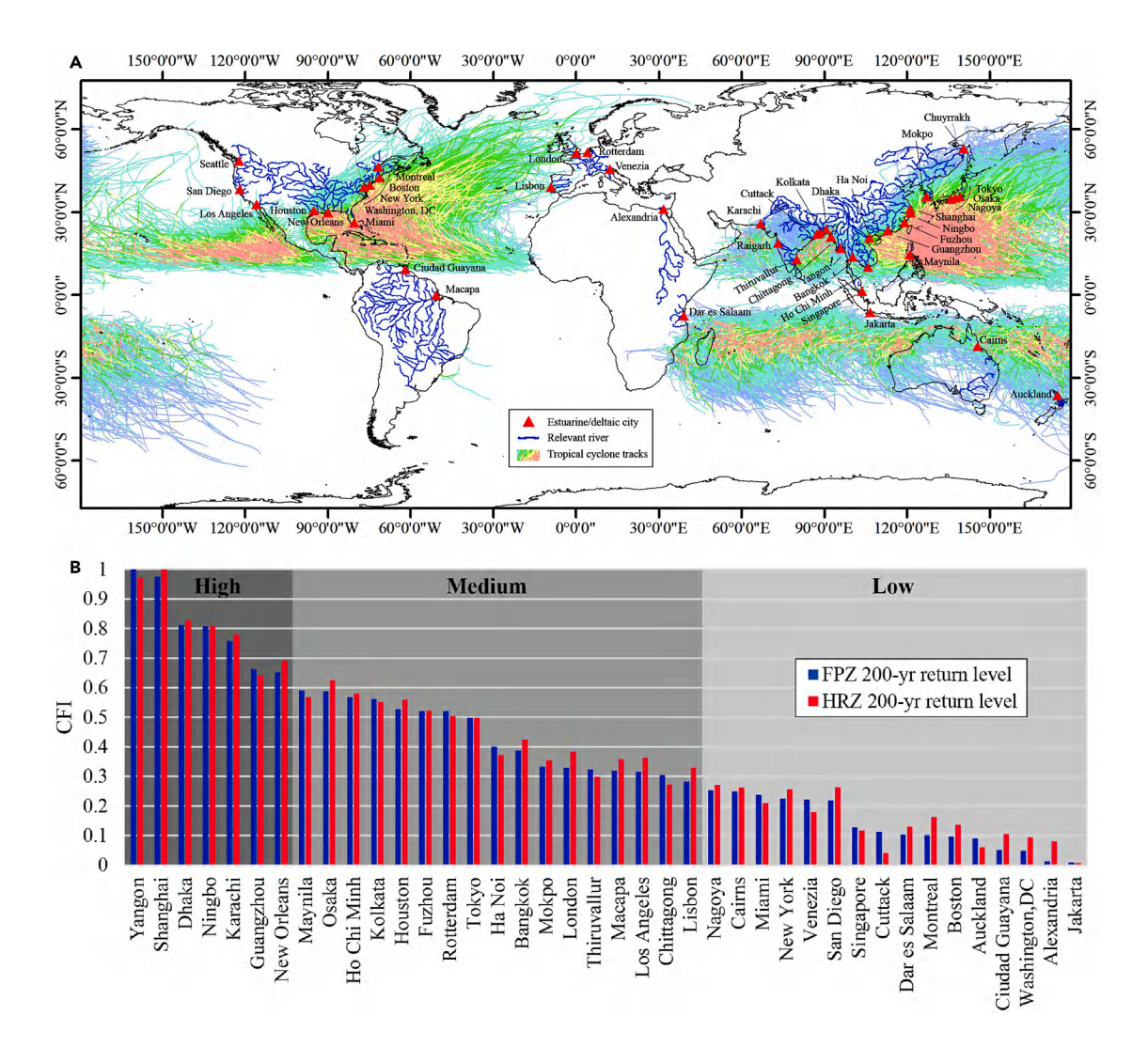


Figure 5. Vulnerability ranking of estuarine/deltaic cities

Ranking of 40 selected estuarine/deltaic cities in the world based on their vulnerability to a 200-year compound-flood hazard. Nine of these cities are located in deltas shown in Figure 4 and Table S4.

(A) Coastal communities influenced by both active cyclone basins and river basins face higher risk of compound floods, with active cyclone basins indicated by historical global tropical and extratropical cyclone tracks during 1842–2020. Each of the 40 selected estuarine/deltaic cities has at least one major river passing through.

(B) Estimates of the relative significance of compound-flood hazard (CFI) for each city, using 200-year return levels of six component proxy indices, i.e., storm surge, tide, precipitation, river discharge, sea-level rise, and land surface subsidence (Figures S17–22). The low, medium, and high compound-flood hazard classes are defined based on three equal classes (0–0.33, 0.33–0.67, and 0.67–1.0).

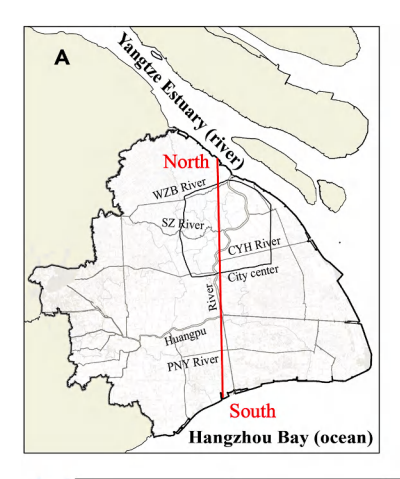
dikes are repaired, as seen in New Orleans after Hurricane Katrina. 19,37 Additionally, the city's low and flat deltaic landscape exacerbates the situation, with Shanghai's elevation progressively falling below compound-flood levels: by 2100, over 90% of the urban area would be submerged during extreme floods, even under the most optimistic emission scenarios (Figure 6C, denoted by the colored lines on the sea). Another key factor contributing to the polder effect is the tidal penetration and interactions with the Huangpu River, which flows through Shanghai's city center and connects to the Yangtze Estuary and Taihu Lake, allowing seawater to penetrate deep into the city (Figure 2). At the same time, river floods from Taihu Lake elevate the WLs in the river, compromising the city's drainage network (Figure 6C)

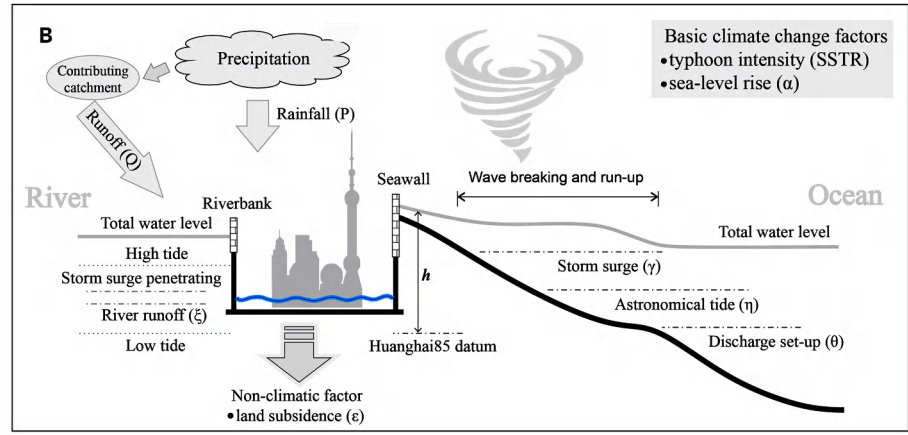
and further amplifying flood risks. Elevated river levels cause direct flooding and pluvial waterlogging due to heavy rainfall (Figure S7) while also blocking gravity-driven drainage (Figure 6C), further intensifying the city's susceptibility to flooding from multiple compound sources.

The global relevance for cities on deltas

Across 40 major estuarine/deltaic cities, more than 300 million people are exposed to compound flooding. 1-3 Many of these cities lie within active cyclone belts, increasing the odds that storm surges, heavy rain, and high river flows coincide (Figure 5A). Using the CFI metric, we find a broad gradient of vulnerability: even places that look less exposed today face sharply rising risk once







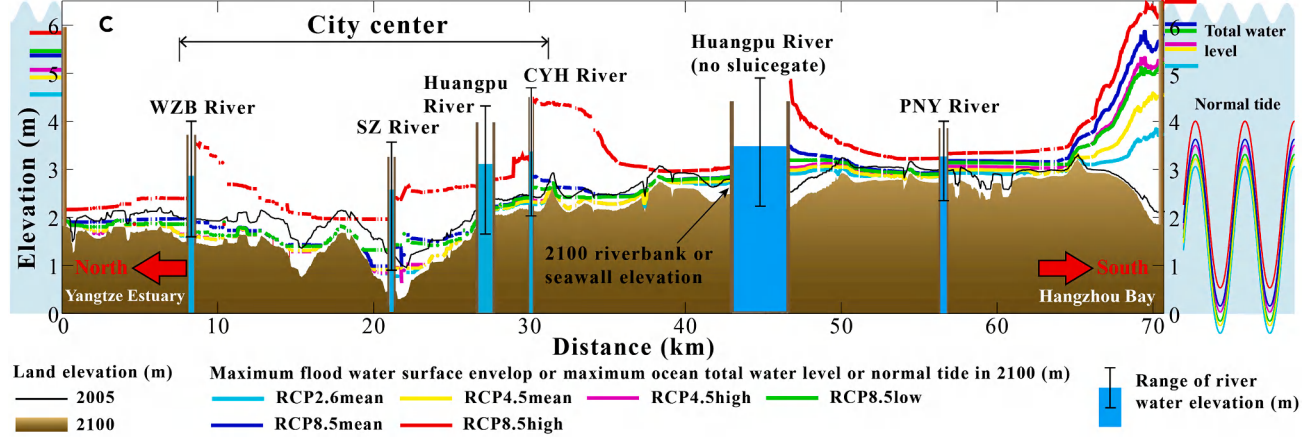


Figure 6. Shanghai: A "sinking polder" city threatened by compound flooding

(A) Sketch map of Shanghai, including a north-south profile through the city center and key rivers.

(B) Schematic synthesis of the polder effect representing all marine, fluvial, and pluvial processes, long-term climate change, and subsidence that contribute to flooding—when overtopping occurs, Shanghai cannot drain naturally.

(C) Overtopping and flood water surface envelope along the profile due to a compound flood projected to the year 2100. Defense heights represent the present condition degraded by subsidence.

SLR and widespread LSS are included (Figure 5B). The seven largest global deltas each contain at least one city where compound flooding is already a major hazard (Figure 4; Table S4). Like Shanghai, these low- to mid-latitude deltas are typically protected by dikes (Figure 4) and built on soft, recently deposited sediments, making them both prone to subsidence^{28,29,32} and sensitive to SLR.^{4,8} While absolute risk varies by site, the same processes recur across deltas—wet-season high river flows and cyclone-driven rainfall and surge acting together over low, defended terrain.^{5,10,44}

To maximize land-use potential, large-scale engineered coastal defenses are a near-universal feature of these large deltas, with variable sophistication and standards (Table S4). This has progressively transformed delta landscapes into polders. For example, the Mekong, Irrawaddy, and GBM deltas use simple earthen infrastructure (e.g., earthen dikes and seawalls), in contrast to the RMS and the Yangtze (e.g., hard-engineered dikes/seawalls and extensive pump capacity). With such interventions, deltas have continued to develop and their populations have expanded, increasing their exposure if flooding

does occur. If the defenses are breached or overtopped, catastrophic flooding can occur in the low-lying polder areas they enclose (Table S4). Examples of such flooding have occurred both in these deltas and elsewhere, with adverse consequences including economic damage and/or loss of life (see Note S3). These events illustrate the potential damage under current conditions, while the Shanghai model shows continued growth of damage in the future. This indicates the importance of understanding and managing flood risk in deltaic cities.

Potential adaptation solutions for compound flooding

As this paper shows, flooding in deltaic cities can be driven by marine, fluvial, or pluvial sources or, at its worst, their combination. Climate-induced SLR and enhanced surges, as well as subsidence, progressively exacerbate this situation. An integrated, multi-layered defense strategy is therefore essential. 30,31,34 In Shanghai, coastal flooding dominates, but rising seas increasingly hamper river drainage and amplify fluvial and pluvial flooding during storm surges. Sluice gates on the Huangpu River's tributaries already temper this interaction; without them, our





worst-case 2100 projections show the FPZ and HRZ expanding by 15% and 53%, respectively (Figure S23). Adding a new storm-surge barrier at the Huangpu River mouth would nearly halve FPZs and HRZs city-wide and cut them by more than 90% along the river (Figure S24). These results underscore the value of sluice gates and surge barriers to mitigate fluvial-sourced floods by reducing marine-fluvial interactions during extreme sea level events—a lesson echoed by the Thames Barrier (London), ⁴⁶ Delta Project and Maeslant Barrier (Rotterdam), ⁴⁵ Lake Borgne Surge Barrier (New Orleans), ³⁸ and MoSE (Venice). ⁴⁷

To address marine flooding, continually raising the elevation of Shanghai's dikes/seawalls may be useful in the short term, but in the long run, it is costly and raises the stakes of catastrophic failure. 16,33,41 A safer path is a multi-layered defense that pairs engineered structures with nature-based buffers: super-levees,48 hybrid dikes that embed vegetated foreshores, 49 double-dike systems with accreting salt-marsh interiors, 6 and -where feasible—strategic retreat to create wider protective zones.³⁸ Restored salt marshes both dampen wave energy and can accrete upwards as sea levels rise and land subsides. 5 To address pluvial flooding, the city should expand low-impact development and sustainable drainage networks, including dike-controlled retention basins, and embed rigorous flood-risk mapping in land-use planning-restricting new construction in HRZs while encouraging flood-proofing in FPZs. Across all hazards, timely warnings and community-based preparedness programs are essential (Table S5). Piloting these integrated measures now will clarify their practical performance and, together with a firm grasp of compound climatic and non-climatic drivers, help secure Shanghai - and other delta megacities - through the 21st century.

METHODS

Coupled numerical modeling system

To quantify the impacts of typhoon-induced compound floods (e.g., multi-hydrometeorological factors, such as storm surge, extreme river discharge, and heavy precipitation) on urban areas within large deltas, we developed a three-set coupled modeling system (AOCM; see supplemental methods) to consider longterm global changes and to transfer regional extreme atmospheric and sea states to local compound-flood predictions. This downscaling procedure allows the effect of long-term climate change (e.g., SLR and SSTR) and anthropogenic impacts (e.g., LSS, including the impacts on both ground elevation and dike height) on urban flood prediction to be directly assessed by considering the key physical processes governing air-sea interactions³⁶ and ocean-coast engagement.¹⁸ The novelty of the methodology is its unique coupling scheme that facilitates the refinement of modeling to a reasonable spatial resolution with high computational efficiency. 18,36,50

In these coupled models, data from each upper-level model are interpolated in space and time to provide boundary arrays for the next-level model (see supplemental methods). Interactions are returned to the upper-level model as feedback, where applicable. ⁴⁰ The coupling scheme comprises three externally linked models (loose coupling) and two internally nested models (intense coupling). For the loose coupling, the cascade proced-

ure is based on a one-way coupling in which the atmosphere model's outputs (precipitation, wind, and pressure) are treated as inputs to the ocean (see I in Figure S31 of supplemental methods) and coast (II in Figure S31 of supplemental methods) models and a two-way coupling in which the ocean and coast models are bidirectionally coupled; thus, the water can flow freely between them (III and IV in Figure S31 of supplemental methods). To achieve this, the WL, consisting of the tide, surge, and wave signals, is spatially aligned with coastal dikes subject to overtopping and temporally interpolated and fed into the coast model at each computational time step. For the intense coupling, both storm waves and tidal currents in the ocean model (V in Figure S31 of supplemental methods) and river discharge and tide propagation in the coast model (VI in Figure S31 of supplemental methods) are dynamically and directly coupled through the processes of wave-current interactions⁴⁰ and backwater effects,⁵¹ respectively. Any resulting dike overtopping flows are formulated as weir flows.3

Next, we use all the models mentioned above for two distinct purposes: (1) hindcasting the historical flood of Typhoon Winnie (no. 9711) and (2) forecasting the reoccurrence of ten historically typical compound events similar to and including Winnie (i.e., 4906: "Gloria"; 5612: "Wanda"; 6207: "Nora"; 7708: "Babe"; 7910: "Judy"; 8114, "Agnes"; 8913: "Kenlora"; 9711: "Winnie"; 0012: "Prapiroon"; and 0509: "Matsa"; see Table S1) under six (to the years 2035, 2050, and 2100) SLR and SSTR scenarios (Table 1). The ten historically extreme compound events, with the same or similar compound factors and component intensities as Typhoon Winnie, are modeled in order to demonstrate the universality of Typhoon Winnie-like compound flooding. All scenario models are run with the same configuration as the control cases, i.e., the observed ten historical typhoon cases, but with 1998 new dikes/seawalls and riverbank defenses (Figure S25B) and with different forcings corresponding to the evolution of ten historical typhoons in 2035, 2050, and 2100, summarized in Table 1. Finally, the real case (which reproduces the flood generated by Typhoon Winnie on August 18, 1997 [Figure S25A], but with the 1997 coastal defense configuration) is used for model calibration and validation (see Figures S25-\$27). The difference between the real and control cases reflects the point that all the coastal defenses in Shanghai were enhanced in a major upgrade in 1998 in response to the Winnie disaster. 16,0

In addition to the control case, which serves as a baseline for reference, the future (to the years 2035, 2050, and 2100) scenarios consider the impacts of anthropogenic land-dike subsidence and climate-driven processes under low- (RCP2.6 mean), medium- (RCP4.5 mean), and high- (RCP8.5 mean) intensity climate change forcings, following the best estimate of the IPCC Fifth Assessment Report⁴² and the projected northwestern pacific typhoon intensity⁵² (Table 1). To investigate the relative importance of SLR and SSTR to future amplified floods, flood areas were tested based on RCP8.5-high scenarios by fixing SLR and increasing or decreasing typhoon intensity for the high and low bound limits of typhoon peak intensity,⁵² and vice versa. The scenario of RCP8.5 high, representing extreme floods using the RCP8.5 high bound limit of SLR and SSTR, is designed to investigate the full range of possible compound floods (Table 1). The SLR range of 0.42-0.92 m covers the 85%



confidence interval range, and the SSTR range of 0.8°C–4.8°C covers the 90% confidence interval range in 2100, based on the beta probability density function. A significance-level analysis of non-compound floods where each factor (SLR, storm surge, precipitation, river discharge, and LSS) is left out is also performed to assess the relative importance of each compound component in isolation (tests 1–5 in Table 1). Further details about the future scenario explanations are provided in Note S2.

For each scenario, the ocean model is run for 40 years (1979–2020) using the updated forcing shown in Table 1. Then, the results are fed into the coast model with different combinations of *SWH*s and *WL*s, with the occurrence probability of future 200-year return period levels (see the stationarity and non-stationarity extreme value analysis using the joint Copula probability calculation in Note S1 and Zhang et al. ³⁵) allowing for the assessment of the future evolution of the present-day 200-year return period flood due to global changes. Then, the modeled flood hazard is defined by the measurement of surface ponding depth (h), where the FPZ is set to $h \geq 0.3$ m, according to FEMA's (Federal Emergency Management Agency of the US) identification of flood hazard zones (www.fema.gov, accessed on February 15, 2022).

Within the FPZ, we set the boundary of the HRZ at $h \geq 1$ m, according to the physical and psychological limitations of human beings in flood situations. The identified FPZs and HRZs are used to evaluate the exposure of property and population at risk based on datasets provided by the National Bureau of Statistics (http://www.stats.gov.cn/, accessed on April 12, 2021). Properties and populations located in the FPZs are considered to be vulnerable to floods, and those exposed to HRZs are considered to be at high risk. The uncertainty of flood risks in FPZs and HRZs can be calculated by combining the appropriate probability distributions of SLR and SSTR, as these are two of the basic model input parameters reflecting global climate changes (Figures 3A and 3B).

CFI assessment model

We developed a global ranking of compound-flood hazards for 40 major estuarine/deltaic cities, focusing on inter-delta differences using a linearized assessment method. In the future (t) and at a given location (x), extreme WLs associated with compound flooding can be expressed by a function of the form

$$h(x,t) = \beta_1 \gamma(x,t) + \beta_2 \eta(x,t) + \beta_3 Q(x,t) + \beta_4 \xi(x,t) + \beta_5 \alpha(x,t) + \beta_6 \varepsilon(x,t),$$
 (Equation 1)

where γ is SSTR-enhanced storm surge, η is tide, Q is precipitation-induced runoff, ξ is river discharge, α is SLR, and ε is LSS, describing the contribution of each flooding driver to the extreme WLs. Using a consistent set of hydrometeorological data, storm surges are estimated in proportion to cyclone wind speed squared ($\gamma \propto U^2$), 4 while runoff Q is estimated using the Soil Conservation Service curve number model from accumulated rainfall P assuming dry antecedent moisture conditions ($Q \propto P$). 55 Hydraulic geometry relations determine flow depth depending on flow discharge at river cross-sections ($\xi \propto \log Q$). 56 The global hazard data rely on long-term IBTrACS_v04 storm track database records since 1842 (www.ncdc.noaa.gov/ibtracs, accessed on April 12, 2021), high-quality Permanent Service for

Mean Sea Level (PSMSL) observations,⁵⁷ hydrological station flow records since 1948,⁵⁸ long-term reanalysis cumulative daily precipitation data (www.pcmdi.llnl.gov/CMIP6, accessed on April 12, 2021), and published global land subsidence data.²⁸ For harmonic tidal range analysis, we used the MATLAB T_Tide package with 28 constituents, which effectively removes stochastic MSL influence.

Using a linearized hypothesis, we develop a dimensionless CFI as a proxy for extreme WL, h(x,t), that links the aforementioned six parameters in a probabilistic way. The effects of each input parameter (here assumed to be statistically independent) incorporate the uncertainties of metrics by appropriate probability distributions with the at-site, T-year (a hazard with 1/T chance of being exceeded in any given year) return level. An appropriate probability law was selected to elaborate the uncertainties of each input parameter in the extreme WL equation h(x,t) from a pool of four marginal distributions, namely the normal distribution, exponential distribution, Weibull distribution, and the generalized extreme value (GEV) distribution. A goodness-of-fit test comparing empirical and theoretical non-exceedance probabilities using the root-mean-square error was applied to identify the best-fitting function. ³⁵ The weighting coefficient $(\beta_i)_{i=1..6}$ for FPZ and HRZ is derived from the Shanghai study. We focus on the 200-year return levels of each input parameter to ensure consistency, where the return level corresponds to the inverse of the yearly exceedance probability (see Figures S17-S22). Finally, the CFI is categorized into three hazard levels-low, medium, and high—based on the compounded flood hazards.

RESOURCE AVAILABILITY

Lead contact

Requests for further information and resources should be directed to the lead contact, Zhijun Dai (zjdai@sklec.ecnu.edu.cn).

Materials availability

This study did not generate new unique materials.

Data and code availability

The long-term IBTrACS_v04 storm track database, covering records since 1842, is available at www.ncdc.noaa.gov/ibtracs, Long-term reanalysis cumulative daily precipitation data can be accessed at www.pcmdi.llnl.gov/CMIP6. Harmonic tidal analysis was performed using the MATLAB T_Tide package. Navigation charts for the lower reach of the Yangtze River were obtained from the Changjiang Waterway Bureau, Ministry of Communications of China, and are available at www.cjhdj.com.cn. Bathymetric data for the continental shelf area were sourced from the GEBCO database, accessible at https:// www.gebco.net/. The digital terrain model (DTM) was constructed based on LiDAR aerial photogrammetry and field measurements, integrating RTK measurements with topographic map data from the Shanghai Institute of Surveying and Mapping, available at https://www.webmap.cn/. Dike/seawall heights, as well as the distribution and structure of sluice gates, were collected through field measurements conducted in 2019. Data on the urban river network, riverbank elevations, and river profiles were provided by the Shanghai Municipal Water Affairs Bureau and the Shanghai Municipal Flood Control Center and can be accessed at https://swj.sh.gov.cn/. The urban flooding model was developed using DHI MIKE software 2016, under a license granted by Shanghai Normal University.

ACKNOWLEDGMENTS

This research is supported by the National Natural Science Key Foundation of China (42430406), the National Natural Science Foundation of China

Please cite this article in press as: Zhang et al., Growing compound-flood risk, driven by both climate change and land subsidence, challenges flood risk reduction in major delta cities, One Earth (2025), https://doi.org/10.1016/j.oneear.2025.101489





(42171282), the National Key R&D Program of China (2023YFE0121200), and the Shanghai Pujiang Program (21PJC096).

AUTHOR CONTRIBUTIONS

Conceptualization, M.Z., R.J.N., T.J.B., and Z.D.; methodology, M.Z., Z.D., and J.W.; resources, M.Z., J.W., and Z.D.; project administration and supervision, M.Z., R.J.N., and Z.D.; writing - original draft, M.Z., R.J.N., A.A., T.J.B., and S.D.; writing - review & editing, all authors.

DECLARATION OF INTERESTS

The authors declare no competing interests.

SUPPLEMENTAL INFORMATION

Supplemental information can be found online at https://doi.org/10.1016/j. oneear.2025.101489.

Received: October 9, 2024 Revised: April 21, 2025 Accepted: September 17, 2025

REFERENCES

- 1. Edmonds, D.A., Caldwell, R.L., Brondizio, E.S., and Siani, S.M.O. (2020). Coastal flooding will disproportionately impact people on river deltas. Nat. Commun. 11, 4741. https://doi.org/10.1038/s41467-020-18531-4.
- 2. Nicholls, R.J., Adger, W.N., Hutton, C.W., and Hanson, S.E. (2020). Deltas in the Anthropocene (Springer Nature), p. 282. https://doi.org/10.1007/ 978-3-030-23517-8.
- 3. Reed, A.J., Mann, M.E., Emanuel, K.A., Lin, N., Horton, B.P., Kemp, A.C., and Donnelly, J.P. (2015). Increased threat of tropical cyclones and coastal flooding to New York City during the anthropogenic era. Proc. Natl. Acad. Sci. USA 112, 12610-12615. https://doi.org/10.1073/pnas.
- 4. Woodruff, J.D., Irish, J.L., and Camargo, S.J. (2013). Coastal flooding by tropical cyclones and sea-level rise. Nature 504, 44-52. https://doi.org/ 10.1038/nature12855.
- 5. Wu, L., Zhao, H., Wang, C., Cao, J., and Liang, J. (2022). Understanding of the Effect of Climate Change on Tropical Cyclone Intensity: A Review. Adv. Atmos. Sci. 39, 205-221. https://doi.org/10.1007/S00376-021-1026-X.
- 6. Zhu, Z., Vuik, V., Visser, P.J., Soens, T., van Wesenbeeck, B., van de Koppel, J., Jonkman, S.N., Temmerman, S., and Bouma, T.J. (2020). Historic storms and the hidden value of coastal wetlands for nature-based flood defence. Nat. Sustain. 3, 853-862. https://doi.org/10.1038/s41893-
- 7. Ao, Z., Hu, X., Tao, S., Hu, X., Wang, G., Li, M., Wang, F., Hu, L., Liang, X., Xiao, J., et al. (2024). A national-scale assessment of land subsidence in China's major cities. Science 384, 301-306. https://doi.org/10.1126/ SCIENCE.ADL4366.
- 8. Nicholls, R.J., Lincke, D., Hinkel, J., Brown, S., Vafeidis, A.T., Meyssignac, B., Hanson, S.E., Merkens, J.L., and Fang, J. (2021). A global analysis of subsidence, relative sea-level change and coastal flood exposure. Nat. Clim. Change 11, 338-342. https://doi.org/10.1038/S41558-021-00993-Z.
- 9. Ganguli, P., and Merz, B. (2019). Trends in Compound Flooding in Northwestern Europe During 1901-2014. Geophys. Res. Lett. 46, 10810-10820. https://doi.org/10.1029/2019GL084220.
- 10. Green, J., Haigh, I.D., Quinn, N., Neal, J., Wahl, T., Wood, M., Eilander, D., de Ruiter, M., Ward, P., and Camus, P. (2024). A Comprehensive Review of Coastal Compound Flooding Literature. Preprint at arXiv. https://doi.org/ 10.48550/arXiv.2404.01321.
- 11. Ikeuchi, H., Hirabayashi, Y., Yamazaki, D., Muis, S., Ward, P.J., Winsemius, H.C., Verlaan, M., and Kanae, S. (2017). Compound simulation of fluvial floods and storm surges in a global coupled river-coast flood

- model: Model development and its application to 2007 Cyclone Sidr in Bangladesh. J. Adv. Model. Earth Syst. 9, 1847-1862. https://doi.org/ 10.1002/2017MS000943.
- 12. Moftakhari, H.R., Salvadori, G., AghaKouchak, A., Sanders, B.F., and Matthew, R.A. (2017). Compounding effects of sea level rise and fluvial flooding. Proc. Natl. Acad. Sci. USA 114, 9785-9790. https://doi.org/10. 1073/pnas.1620325114.
- 13. Wahl, T., Jain, S., Bender, J., Meyers, S.D., and Luther, M.E. (2015). Increasing risk of compound flooding from storm surge and rainfall for major US cities. Nat. Clim. Change 5, 1093-1097. https://doi.org/10.1038/
- 14. Garner, A.J., Mann, M.E., Emanuel, K.A., Kopp, R.E., Lin, N., Alley, R.B., Horton, B.P., Deconto, R.M., Donnelly, J.P., and Pollard, D. (2017). Impact of climate change on New York City's coastal flood hazard: Increasing flood heights from the preindustrial to 2300 CE. Proc. Natl. Acad. Sci. USA 114, 11861-11866. https://doi.org/10.1073/pnas. 1703568114.
- 15. Yu, F., Dong, J., and Ye, L. (2015). Collection of Storm Surge Disasters Historical Data in China 1949-2009 (China Ocean Press). In Chinese.
- 16. Wang, J., Gao, W., Xu, S., and Yu, L. (2012). Evaluation of the combined risk of sea level rise, land subsidence, and storm surges on the coastal areas of Shanghai, China. Clim. Change 115, 537-558. https://doi.org/ 10.1007/s10584-012-0468-7.
- 17. Hsiao, S.C., Fu, H.S., Chen, W.B., Chang, T.Y., Wu, H.L., and Liang, T.Y. (2022). Assessment of future possible maximum flooding extent in the midwestern coastal region of Taiwan resulting from sea-level rise and land subsidence. Environ. Res. Commun. 4, 095007. https://doi.org/10. 1088/2515-7620/ac8f15
- 18. Olbert, A.I., Comer, J., Nash, S., and Hartnett, M. (2017). High-resolution multi-scale modelling of coastal flooding due to tides, storm surges and rivers inflows. A Cork City example. Coast. Eng. 121, 278-296. https:// doi.org/10.1016/j.coastaleng.2016.12.006.
- 19. Xiao, H., Huang, W., and Tao, J. (2009). Numerical modeling of wave overtopping a levee during Hurricane Katrina. Comput. Fluids 38, 991-996. https://doi.org/10.1016/j.compfluid.2008.01.025.
- 20. Torres, J.M., Bass, B., Irza, N., Fang, Z., Proft, J., Dawson, C., Kiani, M., and Bedient, P. (2015). Characterizing the hydraulic interactions of hurricane storm surge and rainfall-runoff for the Houston-Galveston region. Coast. Eng. 106, 7-19. https://doi.org/10.1016/j.coastaleng.2015.09.004.
- 21. Wu, S., Zhou, X., Reyns, J., Yamazaki, D., Yin, J., and Li, X. (2024). Climate change and urban sprawl: Unveiling the escalating flood risks in river deltas with a deep dive into the GBM river delta. Sci. Total Environ. 947, 174703. https://doi.org/10.1016/J.SCITOTENV.2024.174703.
- 22. Qiu, J., Liu, B., Yang, F., Wang, X., and He, X. (2022). Quantitative Stress Test of Compound Coastal-Fluvial Floods in China's Pearl River Delta. Earths Future 10, e2021EF002638. https://doi.org/10.1029/2021EF002638.
- 23. Lin, N., Emanuel, K., Oppenheimer, M., and Vanmarcke, E. (2012). Physically based assessment of hurricane surge threat under climate change. Nat. Clim. Change 2, 462-467. https://doi.org/10.1038/nclimate1389.
- 24. McInnes, K.L., Walsh, K.J.E., Hubbert, G.D., and Beer, T. (2003). Impact of Sea-level Rise and Storm Surges on a Coastal Community. Nat. Hazards 30, 187-207. https://doi.org/10.1023/A:1026118417752.
- 25. Emanuel, K.A. (1987). The dependence of hurricane intensity on climate. Nature 326, 483-485. https://doi.org/10.1038/326483a0.
- 26. Karim, M.F., and Mimura, N. (2008). Impacts of climate change and sealevel rise on cyclonic storm surge floods in Bangladesh. Glob. Environ. Change 18, 490-500. https://doi.org/10.1016/j.gloenvcha.2008.05.002.
- 27. Nicholls, R.J., and Cazenave, A. (2010). Sea-Level Rise and Its Impact on Coastal Zones. Science 328, 1517-1520. https://doi.org/10.2307/
- 28. Herrera-García, G., Ezquerro, P., Tomás, R., Béjar-Pizarro, M., López-Vinielles, J., Rossi, M., Mateos, R.M., Carreón-Freyre, D., Lambert, J., Teatini, P., et al. (2021). Mapping the global threat of land subsidence. Science 371, 34-36. https://doi.org/10.1126/SCIENCE.ABB8549.



- Syvitski, J.P.M., Kettner, A.J., Overeem, I., Hutton, E.W.H., Hannon, M.T., Brakenridge, G.R., Day, J., Vörösmarty, C., Saito, Y., Giosan, L., and Nicholls, R.J. (2009). Sinking deltas due to human activities. Nat. Geosci. 2, 681–686. https://doi.org/10.1038/ngeo629.
- Tessler, Z.D., Vörösmarty, C.J., Grossberg, M., Gladkova, I., Aizenman, H., Syvitski, J.P.M., and Foufoula-Georgiou, E. (2015). Profiling risk and sustainability in coastal deltas of the world. Science 349, 638–643. https://doi.org/10.1126/science.aab3574.
- Becker, M., Seeger, K., Paszkowski, A., Marcos, M., Papa, F., Almar, R., Bates, P., France-Lanord, C., Hossain, M.S., Khan, M.J.U., et al. (2024). Coastal Flooding in Asian Megadeltas: Recent Advances, Persistent Challenges, and Call for Actions Amidst Local and Global Changes. Rev. Geophys. 62, e2024RG000846. https://doi.org/10.1029/2024RG000846.
- Hallegatte, S., Green, C., Nicholls, R.J., and Corfee-Morlot, J. (2013). Future flood losses in major coastal cities. Nat. Clim. Change 3, 802–806. https:// doi.org/10.1038/nclimate1979.
- Welch, A.C., Nicholls, R.J., and Lázár, A.N. (2017). Evolving deltas: Coevolution with engineered interventions. Elementa 5, 49. https://doi. org/10.1525/elementa.128.
- Cao, A., Esteban, M., Valenzuela, V.P.B., Onuki, M., Takagi, H., Thao, N. D., and Tsuchiya, N. (2021). Future of Asian Deltaic Megacities under sea level rise and land subsidence: current adaptation pathways for Tokyo, Jakarta, Manila, and Ho Chi Minh City. Curr. Opin. Environ. Sustain. 50, 87–97. https://doi.org/10.1016/J.COSUST.2021.02.010.
- Zhang, M., Dai, Z., Bouma, T.J., Bricker, J., Townend, I., Wen, J., Zhao, T., and Cai, H. (2021). Tidal-flat reclamation aggravates potential risk from storm impacts. Coast. Eng. 166, 103868. https://doi.org/10.1016/J. COASTALENG.2021.103868.
- Wang, L., Zhang, M., Wen, J., Chong, Z., Ye, Q., and Ke, Q. (2019).
 Simulation of extreme compound coastal flooding in Shanghai. Adv.
 Water Sci. 30, 546–555. https://doi.org/10.14042/j.cnki.32.1309.2019.
 04.010.
- Pistrika, A.K., and Jonkman, S.N. (2010). Damage to residential buildings due to flooding of New Orleans after hurricane Katrina. Nat. Hazards 54, 413–434. https://doi.org/10.1007/s11069-009-9476-y.
- Day, J.W., Boesch, D.F., Clairain, E.J., Kemp, G.P., Laska, S.B., Mitsch, W.J., Orth, K., Mashriqui, H., Reed, D.J., Shabman, L., et al. (2007). Restoration of the Mississippi Delta: Lessons from Hurricanes Katrina and Rita. Science 315, 1679–1684. https://doi.org/10.1126/science. 1137030.
- Gallien, T.W., Sanders, B.F., and Flick, R.E. (2014). Urban coastal flood prediction: Integrating wave overtopping, flood defenses and drainage. Coast. Eng. 91, 18–28. https://doi.org/10.1016/j.coastaleng.2014.04.007.
- Zhang, M., Townend, I., Cai, H., He, J., and Mei, X. (2018). The influence of seasonal climate on the morphology of the mouth-bar in the Yangtze Estuary, China. Cont. Shelf Res. 153, 30–49. https://doi.org/10.1016/j. csr.2017.12.004.
- Du, S., Scussolini, P., Ward, P.J., Zhang, M., Wen, J., Wang, L., Koks, E., Diaz-Loaiza, A., Gao, J., Ke, Q., and Aerts, J.C.J.H. (2020). Hard or soft flood adaptation? Advantages of a hybrid strategy for Shanghai. Glob. Environ. Change 61, 102037. https://doi.org/10.1016/j.gloenvcha.2020. 102037.
- Pachauri, R.K., and Meyer, L.A. (2014). Climate Change 2014: Synthesis Report. Contribution of Working Groups I, II and III to the Fifth Assessment Report of the Intergovernmental Panel on Climate Change (IPCC), p. 151.

- Nicholls, R.J., Hanson, S., Herweijer, C., Patmore, N., Hallegatte, S., Corfee-Morlot, J., Château, J., and Muir-Wood, R. (2008). Ranking Port Cities with High Exposure and Vulnerability to Climate Extremes. In OECD Environment Working Papers, 1 (OECD Publishing). https://doi. org/10.1787/011766488208.
- 44. Kossin, J.P. (2018). A global slowdown of tropical-cyclone translation speed. Nature 558, 104–107.
- Gerritsen, H. (2005). What happened in 1953? The Big Flood in the Netherlands in retrospect. Philos. Trans. A Math. Phys. Eng. Sci. 363, 1271–1291. https://doi.org/10.1098/rsta.2005.1568.
- Beran, M. (1988). Design of Thames Barrier. Nature 336, 104. https://doi. org/10.1038/336104a0.
- Alberti, T., Anzidei, M., Faranda, D., Vecchio, A., Favaro, M., and Papa, A. (2023). Dynamical diagnostic of extreme events in Venice lagoon and their mitigation with the MoSE. Sci. Rep. 13, 10475. https://doi.org/10.1038/S41598-023-36816-8.
- 48. Ohtaa, H., Aoyamab, T., Ochic, S., Shimizud, T., Hamadab, S., and Nakamurab, M. (2017). Alternative Designs of the Super Levee to Protect Below-sea-level Area of Tokyo (BAT) from Flooding. Taiwan Society of Geotechnical Engineering (Ainosco Press), pp. 311–320.
- Temmerman, S., Meire, P., Bouma, T.J., Herman, P.M.J., Ysebaert, T., and De Vriend, H.J. (2013). Ecosystem-based coastal defence in the face of global change. Nature 504, 79–83. https://doi.org/10.1038/ nature12859.
- Chang, T.Y., Chen, H., Fu, H.S., Chen, W.B., Yu, Y.C., Su, W.R., and Lin, L. Y. (2021). An Operational High-Performance Forecasting System for City-Scale Pluvial Flash Floods in the Southwestern Plain Areas of Taiwan. Water 13, 405. https://doi.org/10.3390/w13040405.
- Zhang, M., Yang, H., Tang, Q., Cai, H., Zhu, Z., Feng, A., Luo, M., Gao, H., and Tian, X. (2020). Impacts of secondary and quarter-diurnal tidal species on backwater hydrodynamics in tidal rivers. Adv. Water Resour. 143, 103660. https://doi.org/10.1016/j.advwatres.2020.103660.
- Mei, W., Xie, S.P., Primeau, F., McWilliams, J.C., and Pasquero, C. (2015).
 Northwestern Pacific typhoon intensity controlled by changes in ocean temperatures.
 Sci. Adv. 1, e1500014. https://doi.org/10.1126/sciadv. 1500014.
- Titus, J.G., and Narayanan, V.K. (1995). The Probability of Sea Level Rise (USEPA), p. 186. EPA 230-R95-008.
- Suga, K., Uesaka, T., Yoshida, T., Hamaguchi, K., and Chen, Z. (1995).
 Preliminary Study on Feasible Safe Evacuation in Flood Disaster. Proc. Hydraul. Eng. 39, 879–882. https://doi.org/10.2208/prohe.39.879.
- Michel, C., Andréassian, V., and Perrin, C. (2005). Soil Conservation Service Curve Number method: How to mend a wrong soil moisture accounting procedure? Water Resour. Res. 41, W2011. https://doi.org/10. 1029/2004WR003191.
- Leopold, L.B., and Maddock, T., Jr. (1953). The Hydraulic Geometry of Stream Channels and Some Physiographic Implications (Professional Paper), p. 64. https://doi.org/10.3133/pp252.
- Simon, J.H., Andrew, M., Philip, L.W., Lesley, J.R., Mark, E.T., Elizabeth, B., Peter, R.F., Kathleen, M.G., Svetlana, J., and Jeff, P. (2013). New Data Systems and Products at the Permanent Service for Mean Sea Level. J. Coastal Res. 29, 493–504. https://doi.org/10.2112/JCOASTRES-D-12-00175.1.
- Dai, A., Qian, T., Trenberth, K.E., and Milliman, J.D. (2009). Changes in Continental Freshwater Discharge from 1948 to 2004. J. Clim. 22, 2773– 2792. https://doi.org/10.1175/2008JCLl2592.1.